Journal of Power Sources 345 (2017) 30–40

Contents lists available at ScienceDirect

Journal of Power Sources

journal homepage: www.elsevier.com/locate/jpowsour

Direct methane solid oxide fuel cells based on catalytic partial oxidation enabling complete coking tolerance of Ni-based anodes

Daehee Lee [a, 1], Jaeha Myung [b, 1], Jeiwan Tan [a], Sang-Hoon Hyun [a], John T.S. Irvine [b], Joosun Kim [c], Jooho Moon [a, *]

[a] Department of Materials Science and Engineering, Yonsei University, 50 Yonsei-ro Seodaemun-gu, Seoul, 03722, Republic of Korea
[b] School of Chemistry, University of St. Andrews, North Haugh, KY16 9ST, Scotland, United Kingdom
[c] High-Temperature Energy Materials Research Center, Korea Institute of Science and Technology, Seoul, 02792, Republic of Korea

HIGHLIGHTS

- Direct CH_4 fueled SOFCs operated via catalytic partial oxidation are demonstrated.
- A high performance of 0.74 W cm^{-2} at 550 °C is achieved.
- Enhanced CH_4 conversion suggests a promising internal reforming by CPOX.
- Adsorption dynamics on Ni catalysts is elucidated.

GRAPHICAL ABSTRACT

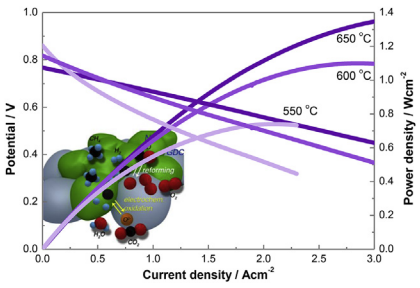

ARTICLE INFO

Article history:
Received 6 October 2016
Received in revised form
31 January 2017
Accepted 1 February 2017

Keywords:
Solid oxide fuel cell
Methane fueling
Ni catalyst
Catalytic partial oxidation
Oxygen exchange kinetics

ABSTRACT

Solid oxide fuel cells (SOFCs) can oxidize diverse fuels by harnessing oxygen ions. Benefited by this feature, direct utilization of hydrocarbon fuels without external reformers allows for cost-effective realization of SOFC systems. Superior hydrocarbon reforming catalysts such as nickel are required for this application. However, carbon coking on nickel-based anodes and the low efficiency associated with hydrocarbon fueling relegate these systems to immature technologies. Herein, we present methane-fueled SOFCs operated under conditions of catalytic partial oxidation (CPOX). Utilizing CPOX eliminates carbon coking on Ni and facilitates the oxidation of methane. Ni-gadolinium-doped ceria (GDC) anode-based cells exhibit exceptional power densities of 1.35 W cm^{-2} at 650 °C and 0.74 W cm^{-2} at 550 °C, with stable operation over 500 h, while the similarly prepared Ni-yttria stabilized zirconia anode-based cells exhibit a power density of 0.27 W cm^{-2} at 650 °C, showing gradual degradation. Chemical analyses suggest that combining GDC with the Ni anode prevents the oxidation of Ni due to the oxygen exchange ability of GDC. In addition, CPOX operation allows the usage of stainless steel current collectors. Our results demonstrate that high-performance SOFCs utilizing methane CPOX can be realized without deterioration of Ni-based anodes using cost-effective current collectors.

© 2017 Elsevier B.V. All rights reserved.

1. Introduction

Mitigating greenhouse gas emissions in view of the increasing global energy demands has become a major priority for our society [1]. A hydrogen economy solely utilizing water-derived hydrogen as

* Corresponding author.
E-mail address: jmoon@yonsei.ac.kr (J. Moon).
[1] These authors contributed equally to this work.

http://dx.doi.org/10.1016/j.jpowsour.2017.02.003
0378-7753/© 2017 Elsevier B.V. All rights reserved.

a universal energy carrier has been regarded as a promising sustainable model. However, the current technologies of hydrogen production using renewable energy sources are not mature enough to provide the required amount of hydrogen [2,3]. In this respect, utilization of the currently available hydrocarbon fuels is still necessary to meet the current and forecast energy demands [3,4]. Specifically, methane (CH_4), as a major constituent of the widely dispersed natural gas, has attracted considerable attention due to its relative abundance and low emission profile [5,6]. However, the exploitation of CH_4 via conventional combustion restricts its conversion efficiency to well below the Carnot efficiency, being accompanied by significant CO_2 emission per unit energy [7,8]. In this respect, the efficient conversion of CH_4 into usable energy is an important prerequisite to satisfy the requirements of both energy demand and low emission.

Solid oxide fuel cells (SOFCs) can help in the clean and efficient utilization of CH_4 due to their unique fuel flexibility [2,4,6]. SOFCs feature oxygen ion conductors as an electrolyte, mediating the oxidation of any fuels, from hydrogen to hydrocarbons, by oxygen ions. In this way, direct utilization of CH_4 in SOFCs without an external reformer can help achieve a maximum theoretical efficiency above 90% and an actual system efficiency of above 65% [2,6], which becomes even higher with combined heat and power (CHP) applications. This can dramatically reduce the CO_2 emission per unit of produced energy without concomitant NO_x generation. Furthermore, the conversion system can be significantly simplified and made more affordable due to the absence of an external reformer, which is a pivotal factor, particularly for small grids or housing systems [4]. Thus, direct CH_4-fueled SOFCs can be an interim system for efficient and low-emission utilization of CH_4 while fully exploiting its current production and transportation infrastructures.

The catalytic and/or electrocatalytic oxidation of CH_4 occurs at the anode of SOFCs composed of a Ni-yttria stabilized zirconia (YSZ) composite, where Ni serves as an (electro)catalyst and an electronic conductor, while YSZ acts as a catalyst support and an oxygen ion conductor. At a typical SOFC operation temperature (600–1000 °C), Ni is capable of reforming CH_4 into syngas (a mixture of H_2 and CO) via catalytic oxidation (i.e., steam reforming, carbon dioxide reforming, or partial oxidation). A mixture of CH_4 and steam is usually fed to the Ni-based anodes, producing syngas that undergoes further electrochemical oxidation, which is known as internal steam reforming [9–11]. However, the deposition of carbonaceous compounds during internal reforming inevitably deactivates the Ni catalyst [11,12]. In particular, CH_4 cracking on the Ni catalyst actively takes place above 700 °C, leading to carbon coking-induced catastrophic failure and restricting long-term operation [13,14]. Moreover, internal steam reforming requires considerable amounts of water to be supplied with fuel to reduce carbon coking, which causes an open circuit voltage (OCV) loss due to fuel dilution [15–17]. In this regard, preventing carbon coking in CH_4-fueled SOFCs has been a major obstacle for their full exploitation.

Significant efforts have been made to address the coking-induced anode deactivation during the internal reforming of CH_4 [6,17–25]. Incorporating CeO_2 or doped CeO_2 into Ni-based anodes helped to oxidize the carbonaceous adsorbates on Ni surfaces owing to the oxygen exchange capability of CeO_2. Since the first demonstration of yttrium-doped ceria (YDC) as a surface carbon oxidation catalyst [26], this approach was combined with a precise control of the CH_4 flow rate to minimize carbon coking, resulting in a further improved power density [27–30]. Similarly, the introduction of a diffusion barrier consisting of partially stabilized ZrO_2 and CeO_2 at the inlet side of the anodes was also suggested to reduce the CH_4 concentration at the anode and increase the reforming rate [31,32]. In addition, the Ni-doped ceria composites have been utilized the anodes for direct utilization of CH_4 in the form of nano-composites or additional metal (Sn, Ru or W)-incorporated composites improving the cell stability and performance [29,33–37]. Despite these efforts, it is generally accepted that Ni-based anodes catalyze CH_4 cracking, inevitably leading to the carbon coking problem, especially in large-scale applications.

In this regard, Ni-free anodes have been developed to avoid the use of the Ni catalyst. Although CeO_2 was suggested as a sole catalyst for CH_4 oxidation, utilizing its lattice oxygen, it suffered from low CH_4 conversion [38,39]. The electrochemical oxidation of CH_4 was demonstrated to electrochemically furnish oxygen ions via Faradaic control of the reaction rate to compensate for the insufficient oxygen supply [17,28,40]. Perovskite-type mixed ionic-electronic conducting oxides such as $La_{1-x}Sr_xCr_{0.5}Mn_{0.5}O_{3-\delta}$, $Sr_2MgMoO_{6-\delta}$, and $La_{1-x}Sr_xTiO_3$ have been developed for this purpose, demonstrating good tolerance toward carbon coking at a high current load condition at which sufficient oxygen ions were provided [41–43]. Despite the remarkable improvements of oxide catalysts, complete CH_4 conversion using this methodology is hardly achievable without the Ni catalyst, considering the low power densities of 0.2–0.44 W cm^{-2} at 800–900 °C obtained for oxide catalyst systems.

From this perspective, the catalytic partial oxidation (CPOX) of CH_4 on a Ni catalyst can be an alternative approach to address the carbon coking issue and simultaneously achieve a high conversion of CH_4. Although there is no consensus on the atomistic mechanism of CH_4 reforming on supported metal catalysts, it is accepted that the carbonaceous adsorbates are readily oxidized by the chemisorbed oxygen species on the metal surface, which are generated from either co-fed oxidants (including H_2O, CO_2, and O_2) or the lattice oxygen supplied by oxide supports [44–46]. Since the surface oxygen is mainly responsible for the elimination of adsorbed carbon, it can be inferred that O_2 should be more effective than other oxidants due to its ease of dissociation. Thus, the CPOX of CH_4, in which half a mole of the O_2 oxidant is supplied to CH_4 for a stoichiometric reaction, can possibly prevent carbon coking. However, the CPOX approach has rarely been applied to SOFC anodes, since the partial pressure of oxygen in the chamber should be maintained below 10^{-18} atm to develop an electrochemical potential gradient that triggers SOFC operation. In addition, the introduction of high concentrations of O_2 into the anode chamber may induce Ni oxidation [47,48]. We have recently demonstrated the optimum microstructures for the CPOX operation of Ni-YSZ anodes [49]. Our work suggested a quantitative evaluation of composite anodes, which was used to study the requirements for continuous and stable operation of the Ni-based anodes under CPOX conditions, representing the possibility of robust CPOX operation without carbon coking and Ni oxidation.

Herein, we demonstrate robust CPOX-based SOFCs fueled by CH_4, circumventing carbon coking and Ni oxidation. The presence of gaseous oxygen in the anode chamber fundamentally prevents carbon coking, while the oxidation of Ni is prevented with the aid of (electro)catalytic reaction controls and oxygen ionic conductors. The resistance of a stainless steel current collector to carbon coking is also demonstrated under CPOX operation, which is essential for the cost-effective design of large-scale SOFC stacks. Electrochemical evaluations in conjunction with *ex situ* surface analyses prove the feasibility of coking-free and oxidation-resistant Ni-based anodes, enabling durable methane-fueled SOFCs. To the best of our knowledge, our novel approach allows us to achieve direct CH_4-fueled SOFCs with long-term stability and the highest performance.

2. Experimental

2.1. Fabrication of unit cells

Anode-supported unit cells consisting of Ni-YSZ ($Y_{0.16}Zr_{0.84}O_{1.92}$)|YSZ|LSM ($La_{0.8}Sr_{0.2}MnO_3$)-YSZ and Ni-GDC ($Gd_{0.2}Ce_{0.8}O_{1.9-\delta}$)|GDC|LSCF ($La_{0.6}Sr_{0.4}Co_{0.8}Fe_{0.2}O_{3-\delta}$)-GDC were fabricated for electrochemical characterization. Ni-YSZ or Ni-GDC (10 wt% of carbon black) anode supports were fabricated by uniaxial pressing and burned-out at 1250 °C for 3 h. The YSZ (TZ8Y, Tosoh Co., Tokyo, Japan) or GDC (Fuel Cell Materials Co., Lewis Center, OH, USA) electrolyte was deposited by dip-coating and sintering at 1400 °C for 3 h. The produced co-sintered pellet was about 19 mm in diameter. The LSM-YSZ or LSCF-GDC cathode (LSM:YSZ = 50:50 w/w, LSCF:GDC = 50:50 w/w) was fabricated by screen printing with a paste of LSM (Fuel Cell Materials Co., Lewis Center, OH, USA) and YSZ powders, or LSCF (Fuel Cell Materials Co., Lewis Center, OH, USA) and GDC powders, respectively, followed by sintering at 950 °C for 4 h. The cell active area was defined as the area of the cathodes, which equaled 1 cm^2.

2.2. Electrochemical characterization

The cell *I-V* characteristics were measured in a four-probe configuration using a potentiostat (Solartron 1287A, Durham, UK). Platinum or SUS 304 mesh and platinum paste (5542, ESL Electroscience, PA, USA) were employed as a current collector. Electrochemical impedance spectroscopy was conducted at a frequency range of 100 kHz–0.1 Hz for all electrochemical characterizations using a potentiostat and frequency analyzer (Solartron 1252, Durham, UK). The anodes were exposed to a 280-sccm total flow rate [STP] of a $CH_4/O_2/N_2$ mixture ($CH_4:O_2:N_2 = 2:1:4$, v/v) and a CH_4/O_2 mixture ($CH_4:O_2 = 2:1$, v/v) at 800 and 650 °C, respectively, while artificial air ($O_2:N_2 = 21:79$, v/v) was supplied to the cathodes during all measurements. The actual cell temperature during the measurements was calibrated by monitoring an additional thermocouple (K-type) located inside the reaction chamber near the cells as shown in Fig. S1 (Supplementary Content).

2.3. Other characterizations

For *ex situ* surface and chemical characterizations, the cells were cooled to room temperature under a flow of Ar. Conductive atomic force microscopy (c-AFM, SPA400, SII, Tokyo, Japan) was performed for a scan area of 50 μm × 50 μm. The conductive area and its perimeter were identified by an image analysis program (ImageJ, National Institutes of Health, Bethesda, MD, USA). X-ray photoelectron spectroscopy (XPS, K-alpha, Thermo Fisher Scientific Inc., Waltham, MA, USA) and elemental analysis (2400 Series II CHNS/O, PerkinElmer, Waltham, MA, USA) were used to characterize the Ni oxidation and carbon deposition behavior of Ni-YSZ and Ni-GDC anodes.

Thin-film Ni samples for X-ray absorption spectroscopy (XAS) experiments were prepared via thermal evaporation (SNTEK, Gyeonggi-do, Republic of Korea) either on the YSZ (001) substrate (Princeton Scientific Co., Princeton, NJ, USA) or GDC film deposited on YSZ (001) by DC magnetron sputtering (SNTEK, Gyeonggi-do, Republic of Korea). During sputtering, the vacuum was maintained at 5 mTorr, with Ar and O_2 supplied to the chamber at flow rates of 30 and 3 cc/min, respectively. XAS experiments were performed in the fluorescence mode at the 10D beamline of PLS II (Pohang Light Sources, Pohang, Republic of Korea). The photon energy was calibrated using the first inflection point of the Ni L_3 edge at 852.7 eV, and the adsorption spectra were subsequently normalized to the adsorption edge jumps.

The composition of effluent gases was analyzed by a gas chromatography (GC) system (Acme 2200, Younglin, Gyeonggi-do, Republic of Korea) equipped with Molesieve 13X and Porapak N columns and a thermal conductivity detector (TCD). The TCD signals were calibrated employing an Ar-balanced (filled) standard gas mixture of CH_4, H_2, CO, CO_2, and N_2 and air. All GC analyses were conducted under a constant total flow rate of the supplied gases.

3. Results and discussion

SOFCs for all electrochemical characterizations were fabricated with an anode-supported cell configuration. LSM-YSZ composite cathodes were utilized for the Ni-YSZ anode-supported cell and LSCF-GDC cathodes were used for the Ni-GDC-supported cell, with the fabrication details described in the Experimental Section. Electrochemical characterization of Ni-YSZ|YSZ|LSM-YSZ cells was performed as a function of feeding gas composition, as shown in Fig. 1. Operation in a flow of mixed gas ($CH_4/O_2/N_2$, $CH_4:O_2:N_2 = 2:1:4$, v/v) results in a maximum power density of 0.91 W cm^{-2} at 800 °C, while using H_2 and CH_4 gases lead to values of 1.06 and 0.78 W cm^{-2}, respectively, as shown in Fig. 1a. Although a slight OCV oscillation is observed (Fig. S2a), stable operation is possible under a flow of mixed gas, with the obtained power density being comparable to the one achieved under H_2 flow and exceeding that produced by feeding CH_4. Electrochemical impedance spectroscopy (EIS) measurements display clear differences in polarization as a function of gas composition (Fig. 1b). EIS spectra recorded under mixed gas conditions reveal a polarization resistance of 0.205 Ω cm^2, while those recorded for H_2 and CH_4 are 0.146 and 0.418 Ω cm^2, respectively. It should be noted that the ohmic resistances (determined by the high-frequency intercept of the polarization arc) obtained at three operation conditions are almost identical: 0.158, 0.153, and 0.150 Ω cm^2 for H_2, mixed gas, and CH_4 feeds, respectively. The major contributor to ohmic resistance is electrolyte resistance, which is dependent only on temperature when the same electrolyte is employed. The similarity of ohmic resistances obtained for three different conditions indicates that the corresponding temperature variation was negligible (even in the case of exothermic CPOX) due to dilution of the mixed gas and the relatively small CPOX enthalpy of CH_4 ($\Delta H_{298} = -36$ kJ/mol). It should be noted that the mixture of CH_4 and O_2 used for CPOX is outside the explosion region, which requires 5–15 vol% CH_4 in air above 650 °C, while typical CPOX conditions feature a CH_4 to O_2 ratio of around two [50]. This safety issue has been addressed by numerous previous works on single-chamber SOFCs [51,52]. Thus, it can be stated that our CPOX operation is safe, as only CH_4 is fueled.

On the other hand, the dependence of polarization resistance on operation conditions can be attributed to the differences in anode polarizations, since the cathodic polarization of LSM-YSZ is constant. The dependence of anodic polarization on gas composition can be attributed to the differences in electrochemical oxidation kinetics arising when the fuel is altered. The electrochemical oxidation of H_2 on metal catalysts is known to exhibit the fastest kinetics among various fuels, resulting in the lowest polarization resistance and the highest power density. On the other hand, the utilization of CH_4 results in distinct polarization responses, irrespective of whether oxygen gas is co-fed into the anode chamber. When only CH_4 is fed to the anode, it undergoes direct electrochemical oxidation by oxygen ions, as expressed in Equation (1) [17,21]:

$$CH_4 + 4O^{2-} \rightarrow CO_2 + 2H_2O + 8e^- \quad (1)$$

This reaction hardly reaches completion, since the

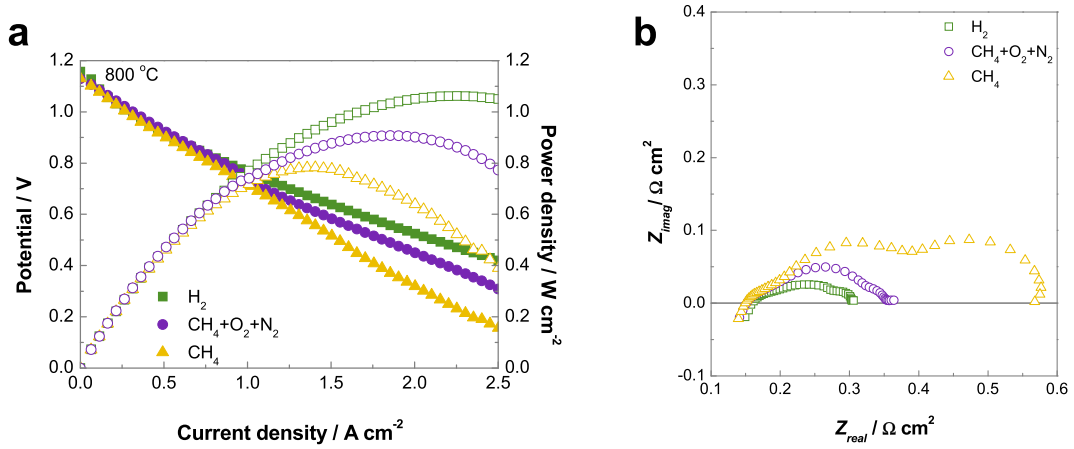

Fig. 1. Electrochemical characterization of Ni-YSZ|YSZ|LSM-YSZ cells at 800 °C as a function of operation conditions. (a) *I-V* characteristics, (b) EIS spectra. Legends in the figure describe the operation conditions: H_2 denotes the feeding of humidified hydrogen gas (80 sccm); CH_4 denotes the feeding of dry methane only (80 sccm); $CH_4 + O_2 + N_2$ denotes operation using a mixture of dry methane, oxygen, and nitrogen (CH_4 80 sccm, O_2 40 sccm, and N_2 160 sccm).

corresponding active sites are restricted to three-phase boundaries (3PBs) that extend ~20 μm from the electrolyte [16]. Therefore, the desorption of surface adsorbates such as CH_x and C in the anode support can be reduced, disturbing the continuous adsorption of CH_4 gas and eventually poisoning the Ni catalyst [53]. Consequently, the direct electrochemical oxidation of CH_4 exhibits relatively sluggish kinetics, which is manifested in the large cell polarization. Conversely, the simultaneous supply of oxygen to Ni anodes leads to the CPOX of CH_4 by the co-adsorbed oxygen atoms as follows:

$$CH_4 + 1/2\ O_2 \rightarrow 2H_2 + CO \quad (2)$$

The dissociated oxygen atoms generate strong oxidants on Ni surfaces, which easily oxidize the adsorbed CH_4 and other intermediates [46,54]. These reactions readily produce electrochemically active products such as H_2 and CO that lower the anodic polarization.

GC analysis of effluent gases revealed that the chemical reforming occurring when oxygen gas is co-fed into the anode chamber indeed took place via the CPOX of CH_4. The exhaust gas composition under OCV conditions represent exclusively the CPOX of CH_4, while that obtained by varying the applied current loads reflects the steady-state levels of CPOX reaction products. The OCV (i.e., zero current load) conversion of CH_4 equaled 54%, with the volume fractions of CH_4 and O_2 being 15.83% and 8.33%, respectively, as shown in Fig. 2a. The ratio of CH_4 to O_2 was 1.90, and was maintained as close as possible to the CPOX stoichiometric ratio (~2), even at increased current loads. This clearly suggests that the conversion of CH_4 occurs via CPOX and stays constant irrespective of the applied current, i.e., it can be regarded as a chemical reforming process. It should be noted that no formation of CO_2 was detected at OCV, implying that CH_4 is converted into syngas via CPOX. In contrast, CO_2 was detected only under an applied current load, indicating the electrochemical utilization of CO. Increasing the applied current load decreases the content of H_2 and CO, while that of CO_2 increases. Such compositional variation of the effluent gases with the applied current can be attributed to the electrochemical consumption of syngas, resulting in the generation of CO_2. The electrochemical conversion was calculated based on the compositions of CO and CO_2 in the effulent gas ($[X_{CO2}/(X_{CO} + X_{CO2})]\%$) and the results were plotted in Fig. 2b. As expected, the electrochemical conversion of CO is enhanced at increased current loadings. These observations confirm that CPOX can efficiently convert CH_4 into

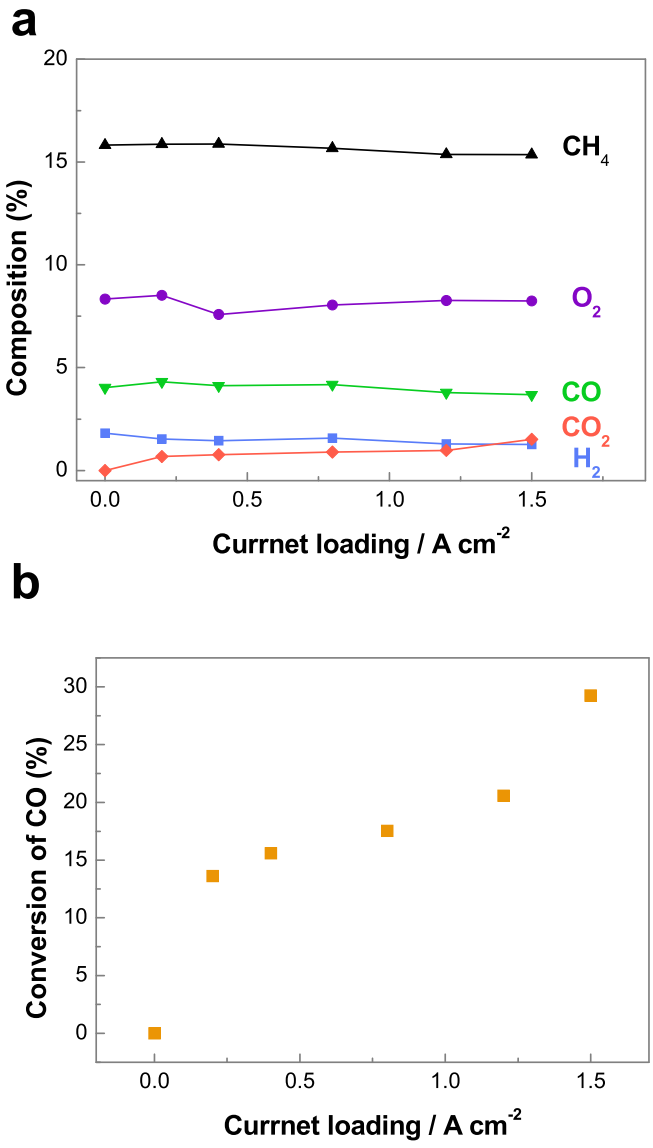

Fig. 2. GC analysis results for effluent gases extracted during operation of Ni-YSZ|YSZ|LSM-YSZ cells at 800 °C. (a) Variation of gas compositions, and (b) electrochemical conversion rate of CO as functions of current loading.

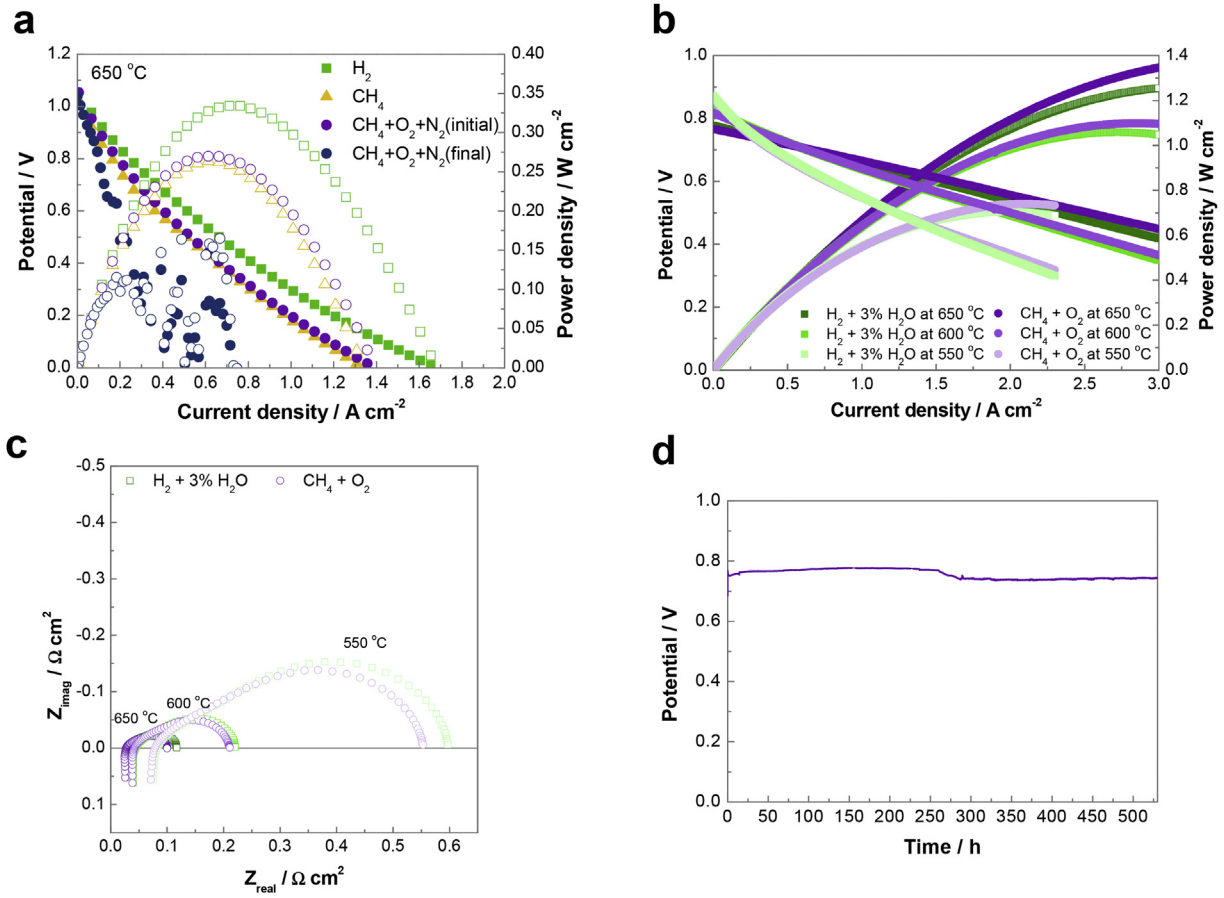

Fig. 3. Electrochemical performance of cells with Ni-GDC and Ni-YSZ anodes at 650 °C. (a) *I-V* characteristics of Ni-YSZ|YSZ|LSM-YSZ cells and (b) Ni-GDC|GDC|LSCF-GDC cells as a function of fuel gas composition. (c) EIS spectra of Ni-GDC cells as a function of fuel gas composition. (d) OCV variation of Ni-GDC cells as a function of fuel gas (CH_4 80 sccm, O_2 40 sccm) exposure at 650 °C.

syngas irrespective of the applied current, making it possible to utilize CH_4 as a fuel in the form of syngas. It should be noted that CPOX is the dominant reforming reaction, as expressed by the constant ratio of $CH_4/O_2 = 1.9$, even when substantial amounts of water vapor are generated by the electrochemical oxidation of H_2 under high current loadings. Operation based on the CPOX of CH_4 at low temperatures (550–650 °C) was evaluated (Fig. 3). Ni-YSZ cells exhibited a maximum power density of 0.27 W cm^{-2} at 650 °C under the CPOX conditions, with the corresponding values of 0.33 and 0.26 W cm^{-2} measured for H_2 and CH_4 feeds, respectively (Fig. 3a). Although the CPOX operation of Ni-YSZ at 650 °C reveals a power density comparable to that initially obtained for H_2, the *I-V* characteristics are completely deteriorated. This phenomenon can be ascribed to the oxidation of Ni by adsorbed oxygen, which deteriorates the catalytic activity and electronic conductivity of the Ni anode [49]. Stable operation under CPOX conditions is achieved by using GDC as an ionic conducting oxide in the composite anode. Maximum power densities of 1.35, 1.10, and 0.74 W cm^{-2} are observed for CPOX operation at 650, 600, and 550 °C, respectively, whereas H_2 operation shows power densities of 1.25, 1.06, and 0.70 W cm^{-2} at 650, 600, and 550 °C, respectively (Fig. 3b). These maximum power densities for the CPOX operation are remarkably higher than those reported previously as compared in Fig. S3. Previous studies have revealed that doped or undoped ceria can catalyze the (electro)chemical oxidation of fuels, with its excellent catalytic activity resulting from the fast transport of ions and electrons [26,39,55,56]. This property and the superior ionic conductivity of GDC are responsible for the remarkable power density achieved under CPOX operation, surpassing that obtained under H_2 operation. On the other hand, the superior performance of the CPOX operation for the Ni-GDC cells may be due to the higher actual flow of fuels during the CPOX operation than the H_2 operation, which is originated from the reason that 1 mol of CH_4 is reformed to 3 mol of fuel gas, i.e. $CO + 2H_2$ upon the CPOX resulting in the accelerated mass transport to the active sites as compare to the supply of 1 mol of H_2. The EIS spectra are consistent with this interpretation, as shown in Fig. 3c. Lower polarization resistances are obtained under CPOX operation (0.072, 0.169, and 0.475 Ω cm^2 at 650, 600, and 550 °C, respectively) than under H_2 operation (0.087, 0.177, and 0.515 Ω cm^2 at 650, 600, and 550 °C, respectively). Notably, the overall arc shapes and peak frequencies of CPOX and H_2 operation are almost identical, indicating that the actual fuel gases utilized in the electrochemically active region might be quite similar. It is generally accepted that the electrochemical oxidation of CH_4 is much more difficult than that of H_2 or CO. Therefore, the similar arc shapes and peak frequencies imply that the atmosphere in the vicinity of the anode active region during CPOX operation consists mainly of H_2 and CO. This observation can be ascribed to the active reforming occurring during CPOX. GC analyses of effluent gases confirm this speculation, as shown in Fig. S4. The conversion of CH_4 is quantified as a function of operation conditions, i.e., CPOX or CH_4-only. It is reasonable to exclude the effect of carbon coking during CPOX, which is nearly zero, as shown in Fig. 4a. The CH_4 conversion ratios during CPOX operation are much higher than

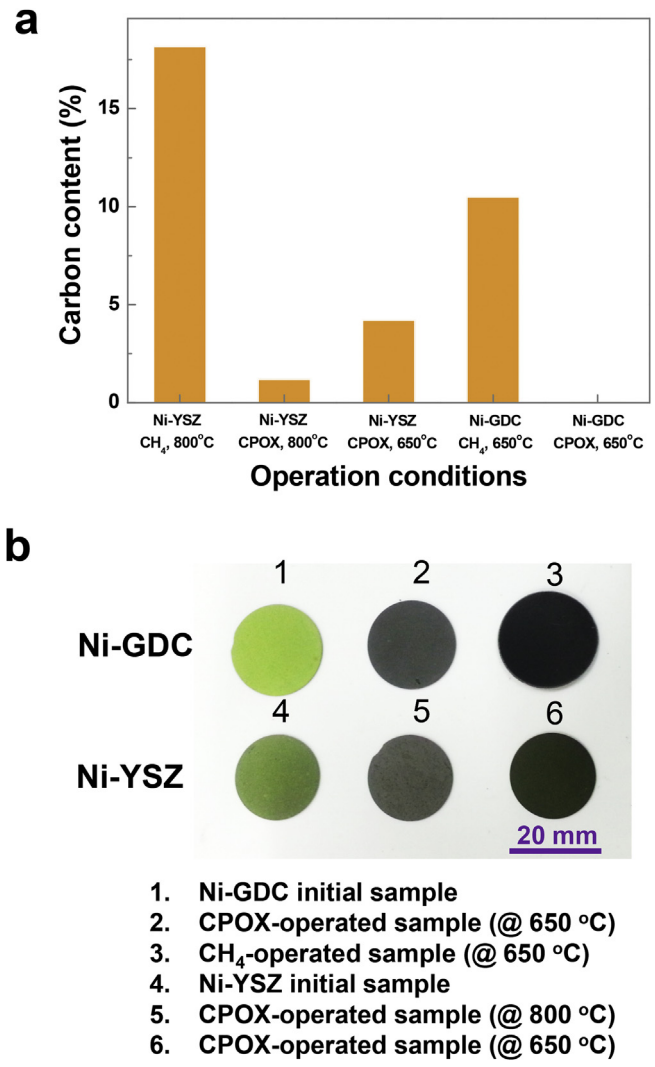

Fig. 4. (a) Carbon content of cells after electrochemical measurements for 5 h, (b) photographs of cells after exposure to the fuel gas denoted in the legend.

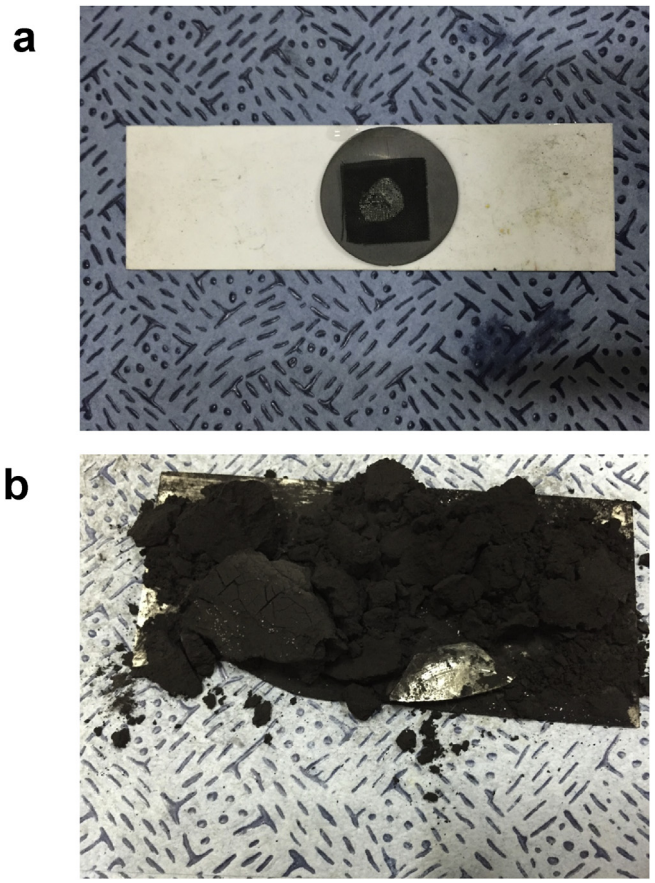

Fig. 5. Photographs of Ni-GDC cells and SUS meshes. (a) Cell and mesh exposed to the mixed gas for 100 h at 650 °C, with individual flow rates as follows: CH_4, 100 sccm; O_2, 50 sccm; and N_2, 200 sccm. (b) Cell and mesh totally disrupted after exposure to the mixture of CH_4 and N_2 (flow rates of 100 and 200 sccm, respectively) for 100 h at 650 °C due to significant carbon coking on the cell and mesh.

those obtained during CH_4-only operation: 48.5% and 45.5% of CH_4 are converted during CPOX operation at 650 and 600 °C, respectively, as shown in Fig. S4a, while only 37.0% and 20.1% of CH_4 are converted under CH_4-only conditions at 650 and 600 °C, respectively (Fig. S4b). Furthermore, a deteriorated CH_4 conversion is observed during CH_4-only operation at 600 °C, accompanied by a gradual OCV drop, as shown in Fig. S4c. This degradation can be ascribed to significant carbon coking during the CH_4-only operation in absence of O_2. These observations allow us to conclude that the low polarization during CPOX operation originates from the high CH_4 reforming rate under CPOX conditions.

A long-term CPOX operation stability test was performed using a Ni-GDC cell (Fig. 3d). An OCV degradation of ~0.91% is observed after 530 h of operation. Note that the long-term stability of the CH_4-fueled SOFCs can be further improved by applying the higher polarization current [40], therefore, the observed stability of the CPOX operation in this study can be regarded as the best performance as compared with previous works in Table S1. In contrast, operation under CH_4 feeding conditions shows a drastic OCV degradation after 5 h, caused by carbon coking (Fig. S2b). After the measurements, the cells were subjected to elemental analysis to characterize the deposition of carbon, as shown in Fig. 4a and Table S2. The carbon content of the CPOX-operated cell equals 0.02 wt%, while that of the CH_4-operated one is 10.49 wt%. The deposition of carbon on Ni surfaces can result in the formation of nickel carbides, which is accompanied by volume expansion and the generation of cracks (Fig. 4b). The small amount of carbon detected for the CPOX-operated cell indicates the efficient prevention of carbon deposition by the presence of oxygen under CPOX conditions. To additionally confirm the absence of carbon coking on CPOX-operated current collectors, stainless steel (SUS) 304 mesh was employed as a current collector for Ni-GDC cells and was aged under both CH_4-only and CH_4-O_2 mixed gas conditions. The SUS meshes were attached to the anode side using Ag paste and were subsequently exposed to the same flow rate of CH_4 (100 sccm) at 650 °C for 100 h. The SUS mesh aged under CH_4-O_2 mixed gas conditions shows insignificant carbon coking, resulting in a weight gain of 2.03%, as shown in Fig. 5a. However, substantial carbon coking of the SUS 304 mesh is observed for the cell aged under CH_4-only conditions, leading to total cell and mesh disruption due to the formation of carbides, as shown in Fig. 5b. The SUS mesh microstructures aged under CPOX conditions exhibit no significant deformation or pitting, with particulate carbons observed only at the surface region, as shown in Figs. S5a and S5b. Energy dispersive X-ray spectroscopy (EDX) mapping of the corresponding cross-section reveals that particulate carbons are generated only at the surfaces, while the bulk SUS mesh retains its metallic character, as depicted in Fig. S5d. Note that filamentous growth of carbon

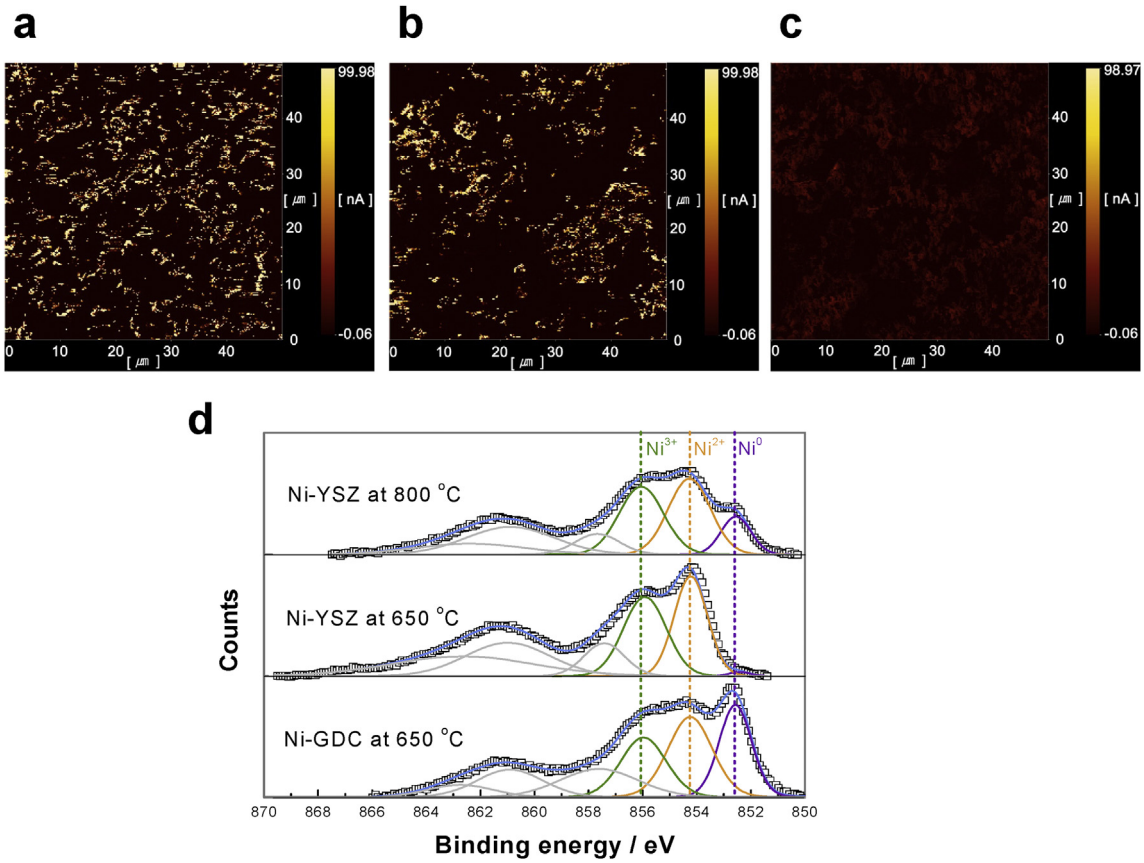

Fig. 6. *Ex situ* surface analysis results for Ni-GDC and Ni-YSZ anodes exposed to the mixture of CH_4, O_2, and N_2 at different temperatures. c-AFM maps of (a) Ni-GDC anode at 650 °C, (b) Ni-YSZ anode at 800 °C, and (c) Ni-YSZ anode at 650 °C. (d) XPS spectra of Ni-GDC and Ni-YSZ anodes after operation.

generally leads to catastrophic deformation of metals; however, the carbons generated under CPOX conditions exhibit particulate growth, implying retarded surface diffusion and carbon species growth, thereby preventing SUS mesh failure. On the other hand, partial oxidation of metals is observed in the surface region, which may cause the small cracks shown in Fig. S5c. Previously, we have demonstrated stable long-term 500-h operation with dry CH_4 fuel in the absence of additional oxidant gas, achieved with the help of the synthesized nanocomposite Ni-GDC/GDC powders [29]. Similarly, long-term 120-h operation with a CH_4-CO_2 mixture has been reported for alumina-modified Ni-YSZ powders [57], and a samarium-doped ceria (SDC)-infiltrated Ni-YSZ anode allowed a long-term operation of 450 h using CH_4 [30]. Despite these successful demonstrations, stable long-term operation was possible only with a precisely controlled low CH_4 flow rate and a gold current collector for preventing carbon coking, which is difficult to achieve in practical applications utilizing large-area cell stacks. Our observations of the SUS 304 mesh clearly show that CPOX operation allows to employ stainless steel as a cost-effective current collector without significant carbon coking, which otherwise leads to the catastrophic failure of SOFCs [58].

To understand the origin of the long-term stability of the Ni-GDC anode, *ex situ* surface analyses by c-AFM and XPS were performed for CPOX-operated cells, including Ni-GDC at 650 °C, Ni-YSZ at 800 °C, and Ni-YSZ at 650 °C. The conductive anode surface areas measured by c-AFM are displayed in Fig. 6a–c. The bright areas of the images represent conductive areas, with conductivity scaling with brightness. The conductive maps of Ni-GDC at 650 °C and Ni-YSZ at 800 °C show distinctive conductive areas with maximum brightness, ascribed to metallic Ni, while these areas exhibit lower conductivity for Ni-YSZ at 650 °C, as expressed by darker regions. This result indicates that Ni in the Ni-YSZ anode undergoes significant oxidation during CPOX operation at 650 °C. Therefore, the drastic degradation of power density at 650 °C can be attributed to the deactivation of Ni catalysts by oxidation. On the other hand, Ni-YSZ CPOX operated at 800 °C is only partially oxidized, while Ni-GDC operated at 650 °C remains as metallic Ni. The area fraction of conductive regions (17.63 ± 0.72%) is higher for Ni-GDC at 650 °C than for Ni-YSZ at 800 °C (10.30 ± 1.06%). This variable extent of Ni oxidation accounts for different cell stabilities, with Ni-GDC showing stable operation without little degradation and Ni-YSZ exhibiting a slight oscillation of OCV. Ni $2p_{3/2}$ XPS spectra shows consistent trends in the oxidation states of Ni, as plotted in Fig. 6d. The peaks observed in Ni $2p_{3/2}$ spectra at binding energies of 852.6, 854.6, and 856.1 eV can be assigned to Ni^0, Ni^{2+}, and Ni^{3+}, respectively [59,60]. The fraction of the Ni^0 peak of Ni-GDC at 650 °C is 32.26%, whereas those of Ni-YSZ at 800 °C and Ni-YSZ at 650 °C are 15.30% and 1.20%, respectively. These observations imply that Ni exists predominantly in its metallic state in Ni-GDC at 650 °C, while it is partially oxidized at 800 °C in Ni-YSZ and undergoes significant oxidation when the operation temperature is lowered to 650 °C.

The partial oxidation of Ni in Ni-YSZ at 800 °C can be explained in terms of the 3PB/two-phase boundary (2PB) ratios of electrodes, with 2PBs determined by the bright areas and 3PBs defined as the perimeter of these areas. This ratio equaled 0.97 m^{-1} for Ni-YSZ, as determined by image analysis (Fig. 7a–c). In our previous work [49], the 3PB/2PB ratio played a key role in determining the CPOX

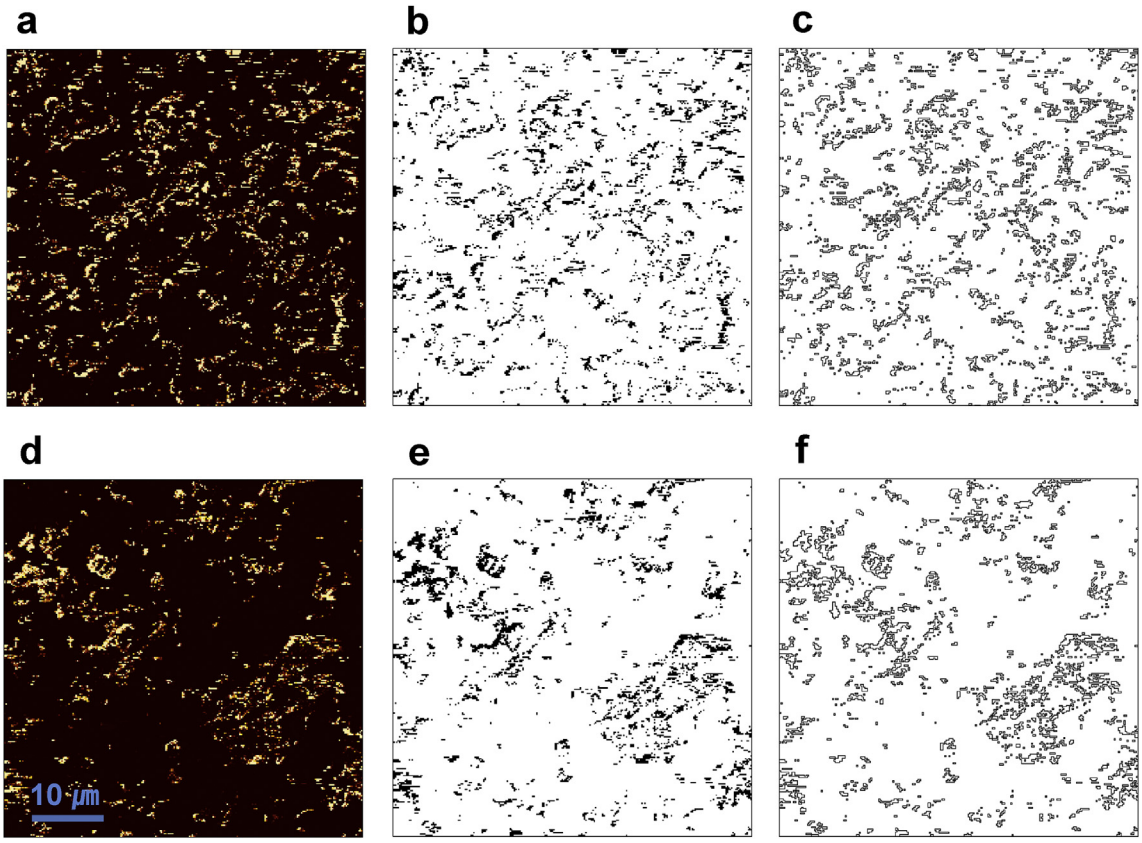

Fig. 7. c-AFM images and image analyses procedures for Ni-GDC and Ni-YSZ anodes exposed to the mixture of CH_4, O_2, and N_2 gases. Analysis of the c-AFM images using the ImageJ program provided the conductive area and its perimeter, corresponding to the 2PB region and 3PB length, respectively. (a) c-AFM image of the Ni-GDC anode after exposure at 650 °C, (b) area fraction of bright regions for the Ni-GDC anode, (c) perimeter of bright regions, (d) c-AFM image of the Ni-YSZ anode after exposure at 800 °C, (e) area fraction of bright regions for the Ni-YSZ anode, and (f) perimeter of bright regions. All images are at the same scale.

kinetics, with CPOX activity maintained by the prompt elimination of surface adsorbates such as CH_x, C, and O in accordance with the electrochemical oxidation of syngas. Sufficient 3PB/2PB ratios above ~1.08 m^{-1} could accelerate the consumption of adsorbates, leading to a continuous CPOX reaction without carbon coking or Ni oxidation [49]. The ratio of Ni-YSZ (0.97 m^{-1}) is close to the value at which the repetitive oxidation and reduction of Ni occur (0.99 m^{-1}), leading to the OCV oscillation depicted in Fig. S2a. Therefore, some parts of Ni in Ni-YSZ at 800 °C are oxidized, as detected by XPS and c-AFM analyses. Ni-GDC anodes show a 3PB/2PB ratio of 1.12 m^{-1} (Fig. 7d and e), fulfilling the minimum criterion of stable CPOX operation without Ni oxidation and carbon coking.

On the other hand, the utter failure of Ni-YSZ at an operation temperature of 650 °C cannot be explained solely by the 3PB/2PB ratio, since complete disruption occurs only at a much lower 3PB/2PB ratio of ~0.7 m^{-1} [49]. In other words, the deterioration of Ni-YSZ cells due to Ni oxidation cannot be explained in terms of electrode microstructures. This consideration suggests that the ion-conducting oxides in the composite electrode, i.e., GDC and YSZ, play a role in determining the oxidation stability of Ni during the CPOX of CH_4. In this regard, the influence of the ion-conducting oxide type in the composite electrode on Ni oxidation was studied by XAS. For transition metal elements, the pre-edge structures provide detailed information on the *d*-band structure. Two or three pre-edge sub-peaks (denoted A_i) appear at energies well below that of the main edge (usually 15 eV below) and are assigned to a $1s \rightarrow 3d^{(n+1)}$ transition, where n is the initial number of *d*-orbital electrons and $(n+1)$ represents the number of excited electrons in the final state [61]. Since nickel oxidation is sensitive to the structure of its *d*-level, which hosts electrons interacting with oxygen 2*p* levels, it is necessary to determine whether the electronic structures of Ni/GDC and Ni/YSZ are different. Thin Ni films fabricated on either YSZ or GDC by thermal evaporation were employed for XAS studies to exclude geometrical irregularity such as porosity and tortuosity. The corresponding Ni *K*-edge spectra are plotted in Fig. 8a, with Ni on YSZ or GDC exhibiting identical structures. Soft X-ray total electron yield studies of Ni $L_{3,2}$ edges also show a similar structure for both Ni/YSZ and Ni/GDC, as shown in Fig. 8b. Ni $L_{3,2}$ edge structures for both YSZ and GDC are similar to that of Ni foil. In contrast, the oxidation of Ni is accompanied by the appearance of the L_3 edge shoulder and the splitting of the L_2 edge, as seen for the NiO reference sample. Therefore, we conclude that Ni-YSZ and Ni-GDC composites exhibit no difference in the chemical state of Ni, which is present in its metallic state in both samples.

This XAS result emphasizes another example of how the type of the ion-conducting oxide in the Ni composite anode is responsible for the robust CPOX operation. GDC not only exhibits better ionic conductivity than YSZ, but also shows remarkable (electro)catalytic activity due to the facile transport of oxygen ions and electrons, particularly under the reducing atmosphere of the anode chamber. The excellent catalytic activity of doped and undoped ceria has been reported in previous studies, where ceria showed a catalytic activity exceeding that of conventional metal catalysts such as Pt and Ni [55,56]. Due to the superior (electro)catalytic activity of ceria, it has been suggested for use as a CPOX catalyst to achieve stable conversion kinetics without metal catalyst poisoning by carbon coking [26,39,62]. Based on these considerations, the

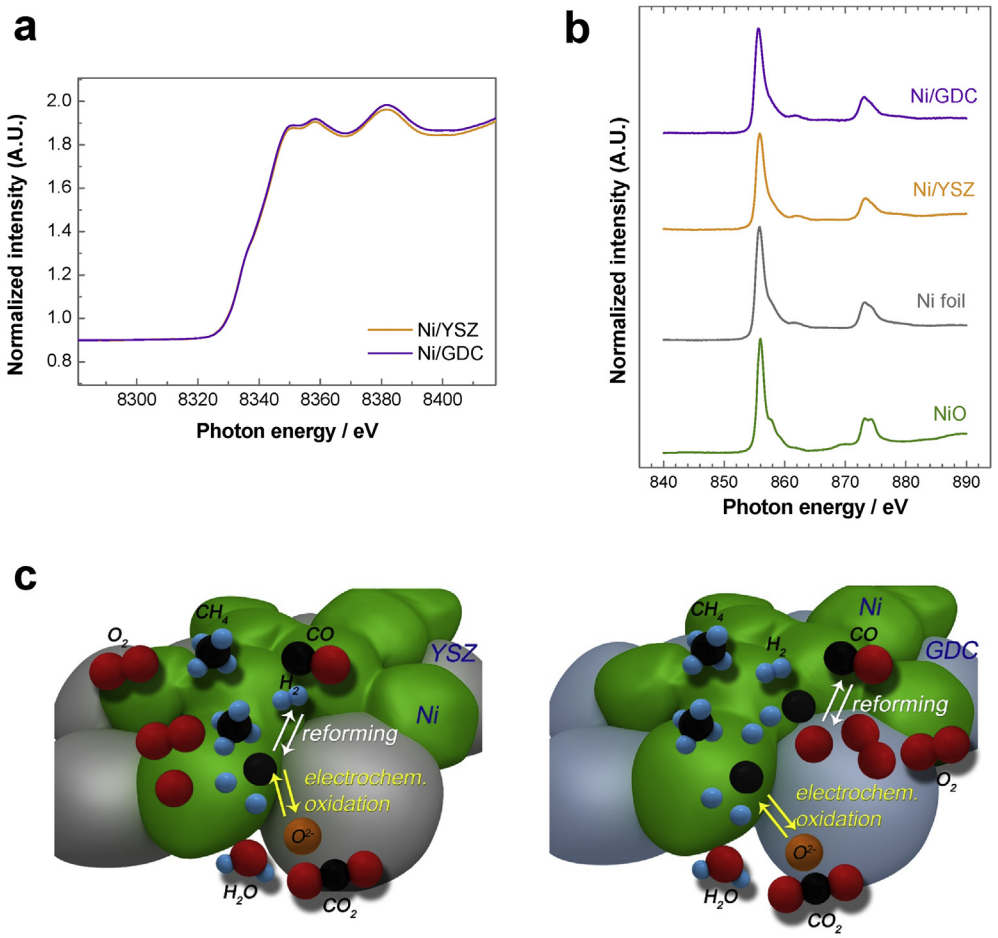

Fig. 8. XAS spectra of Ni thin films grown on either YSZ (100) single crystals or GDC thin film which was epitaxially grown on YSZ (100) single crystals, and the oxidation mechanisms proposed for CPOX operation. (a) Ni *K* edge spectra of Ni on YSZ and GDC. (b) Ni $L_{3,2}$ edge spectra of various Ni samples. (c) Schematic illustrations of surface reactions on Ni-GDC and Ni-YSZ anodes. For the Ni-YSZ anode, both CH_4 and O_2 are favorably adsorbed on Ni surfaces, with the adsorbed oxygen oxidizing Ni, whereas O_2 is preferentially adsorbed on GDC surfaces and CH_4 is predominantly adsorbed on Ni surfaces, maintaining the metallic nature of Ni surfaces.

proposed surface reaction models of the Ni-GDC and Ni-YSZ anodes are illustrated in Fig. 8c. During the CPOX of CH_4 on the Ni-GDC anode surface, CH_4 is predominantly adsorbed on Ni surfaces, while oxygen prefers GDC surfaces due to the partial reduction of ceria under the reducing conditions of the anode chamber. Subsequently, the adsorbed carbon species are easily oxidized by the oxygen readily supplied by ceria, so that the anode 3PBs act as active sites for CH_4 oxidation, regardless of the presence of electrochemically replenished oxygen ions from the electrolyte. If the Ni-GDC anode has sufficiently large 3PBs, CPOX occurs continuously, effectively removing adsorbates and products and preventing the oxidation of Ni. On the contrary, in case of the YSZ support for Ni, O_2 is preferentially adsorbed on Ni surfaces due to its inherently high electronegativity. This leads to the oxidation of Ni surfaces by the surface-bound oxygen, gradually degrading the (electro)catalytic activity even when a high 3PB/2PB ratio is maintained. Our results highlight the critical role of the ion-conducting oxide in composite anodes for preventing catalytic activity degradation due to oxidation or carbon coking.

4. Conclusions

In this study, durable high-performance direct CH_4 SOFCs were successfully demonstrated. The presence of oxidants during the CPOX of CH_4 hindered the deposition of carbon on the nickel catalyst and facilitated the oxidation of CH_4 fuel, which reduced polarization resistance and increased CH_4 conversion, as compared to the CH_4-only case. Ni-GDC cells exhibited maximum power densities of 1.35 and 0.74 W cm^{-2} at 650 and 550 °C, respectively, which were maintained for over 500 h without degradation, while Ni-YSZ cells exhibited a value of 0.27 W cm^{-2} at 650 °C, with subsequent cell degradation. In addition, the stability of a cost-effective stainless steel current collector under CPOX conditions was confirmed. Surface and electronic structure analyses of the Ni catalyst were performed as a function of the ion-conducting oxide type in the composite anode, utilizing XPS, c-AFM, and XAS. The obtained results suggested that the use of GDC as an ion-conducting oxide in the composite electrode prevented the deactivation of Ni catalysts owing to its excellent oxygen exchange capability, which ensured that the activity of the CPOX reaction sites was preserved and excluded the oxidation or carbon coking-induced poisoning of Ni. This novel strategy utilizing CH_4 co-fed with oxygen demonstrates the outstanding performance of CH_4-fueled SOFCs, which can help to realize readily available alternative power generation systems using the current infrastructures for CH_4. Our findings also provide the design rules for ensuring stable long-term operation under CPOX conditions at low temperatures.

Acknowledgements

This work was supported by the Samsung Research Funding Center of Samsung Electronics, project number SRFC-MA1501-03.

Appendix A. Supplementary data

Supplementary data related to this article can be found at http://dx.doi.org/10.1016/j.jpowsour.2017.02.003.

References

[1] R.B. Jackson, J.G. Canadell, C. Le Quéré, R.M. Andrew, J.I. Korsbakken, G.P. Peters, N. Nakicenovic, Reaching peak emissions, Nat. Clim. Change 6 (2015) 7–10, http://dx.doi.org/10.1038/nclimate2892.
[2] E.D. Wachsman, K.T. Lee, Lowering the temperature of solid oxide fuel cells, Science 334 (2011) 935–939, http://dx.doi.org/10.1126/science.1204090.
[3] M. Schrope, Which way to energy utopia? Nature 414 (2001) 682–684, http://dx.doi.org/10.1038/414682a.
[4] E.D. Wachsman, C.A. Marlowe, K.T. Lee, Role of solid oxide fuel cells in a balanced energy strategy, Energy Environ. Sci. 5 (2012) 5498–5509, http://dx.doi.org/10.1039/C1EE02445K.
[5] World Energy Outlook 2011 Special Report - Are We Entering a Golden Age of Gas?, International Energy Agency, 2011.
[6] W. Wang, C. Su, Y. Wu, R. Ran, Z. Shao, Progress in solid oxide fuel cells with nickel-based anodes operating on methane and related fuels, Chem. Rev. 113 (2013) 8104–8151, http://dx.doi.org/10.1021/cr300491e.
[7] S.O. Akansu, Z. Dulger, N. Kahraman, T.N. Veziroğlu, Internal combustion engines fueled by natural gas—hydrogen mixtures, Int. J. Hydrog. Energy 29 (2004) 1527–1539, http://dx.doi.org/10.1016/j.ijhydene.2004.01.018.
[8] H. McJeon, J. Edmonds, N. Bauer, L. Clarke, B. Fisher, B.P. Flannery, J. Hilaire, V. Krey, G. Marangoni, R. Mi, K. Riahi, H. Rogner, M. Tavoni, Limited impact on decadal-scale climate change from increased use of natural gas, Nature 514 (2014) 482–485, http://dx.doi.org/10.1038/nature13837.
[9] Y.J. Kim, H.M. Lee, H.-T. Lim, Degradation comparison of hydrogen and internally reformed methane-fueled solid oxide fuel cells, J. Korean Ceram. Soc. 53 (2016) 483–488, http://dx.doi.org/10.4191/kcers.2016.53.5.483.
[10] T. Horita, N. Sakai, T. Kawada, H. Yokokawa, M. Dokiya, Oxidation and steam reforming of CH_4 on Ni and Fe anodes under low humidity conditions in solid oxide fuel cells, J. Electrochem. Soc. 143 (1996) 1161–1168, http://dx.doi.org/10.1149/1.1836613.
[11] A.L. Dicks, K.D. Pointon, A. Siddle, Intrinsic reaction kinetics of methane steam reforming on a nickel/zirconia anode, J. Power Sources 86 (2000) 523–530, http://dx.doi.org/10.1016/S0378-7753(99)00447-4.
[12] J. Macek, B. Novosel, M. Marinsek, Ni-YSZ SOFC anodes - minimization of carbon deposition, J. Eur. Ceram. Soc. 27 (2007) 487–491, http://dx.doi.org/10.1016/j.jeurceramsoc.2006.04.107.
[13] C.M. Finnerty, N.J. Coe, R.H. Cunningham, R.M. Ormerod, Carbon formation on and deactivation of nickel-based/zirconia anodes in solid oxide fuel cells running on methane, Catal. Today 46 (1998) 137–145, http://dx.doi.org/10.1016/S0920-5861(98)00335-6.
[14] R.J. Gorte, S. Park, J.M. Vohs, C. Wang, Anodes for direct oxidation of dry hydrocarbons in a solid-oxide fuel cell, Adv. Mater. 12 (1465–1469) (2000), http://dx.doi.org/10.1002/1521-4095(200010)12:19<1465::AID-ADMA1465>3.0.CO;2–9.
[15] T. Takeguchi, R. Kikuchi, T. Yano, K. Eguchi, K. Murata, Effect of precious metal addition to Ni-YSZ cermet on reforming of CH_4 and electrochemical activity as SOFC anode, Catal. Today 84 (2003) 217–222, http://dx.doi.org/10.1016/S0920-5861(03)00278-5.
[16] N. Laosiripojana, S. Assabumrungrat, Catalytic steam reforming of methane, methanol, and ethanol over Ni/YSZ: the possible use of these fuels in internal reforming SOFC, J. Power Sources 163 (2007) 943–951, http://dx.doi.org/10.1016/j.jpowsour.2006.10.006.
[17] M. Mogensen, K. Kammer, Conversion of hydrocarbons in solid oxide fuel cells, Annu. Rev. Mater. Res. 33 (2003) 321–331, http://dx.doi.org/10.1146/annurev.matsci.33.022802.092713.
[18] B.C.H. Steele, Survey of materials selection for ceramic fuel cells II. Cathodes and anodes, Solid State Ion 86–88 (Part 2) (1996) 1223–1234, http://dx.doi.org/10.1016/0167-2738(96)00291-3.
[19] N.P. Brandon, S. Skinner, B.C.H. Steele, Recent advances in materials for fuel cells, Annu. Rev. Mater. Res. 33 (2003) 183–213.
[20] A. Atkinson, S. Barnett, R.J. Gorte, J.T.S. Irvine, A.J. McEvoy, M. Mogensen, S.C. Singhal, J. Vohs, Advanced anodes for high-temperature fuel cells, Nat. Mater. 3 (2004) 17–27, http://dx.doi.org/10.1038/nmat1040.
[21] S. McIntosh, R.J. Gorte, Direct hydrocarbon solid oxide fuel cells, Chem. Rev. 104 (2004) 4845–4866, http://dx.doi.org/10.1021/cr020725g.
[22] J.B. Goodenough, Y.-H. Huang, Alternative anode materials for solid oxide fuel cells, J. Power Sources 173 (2007) 1–10, http://dx.doi.org/10.1016/j.jpowsour.2007.08.011.
[23] R.J. Gorte, J.M. Vohs, Catalysis in solid oxide fuel cells, Annu. Rev. Chem. Biomol. Eng. 2 (2010) 1–22.
[24] W. Wang, H. Zhu, G. Yang, H.J. Park, D.W. Jung, C. Kwak, Z. Shao, A NiFeCu alloy anode catalyst for direct-methane solid oxide fuel cells, J. Power Sources 258 (2014) 134–141, http://dx.doi.org/10.1016/j.jpowsour.2014.02.008.
[25] W. Wang, C. Su, R. Ran, H.J. Park, C. Kwak, Z. Shao, Physically mixed LiLaNi–Al_2O_3 and copper as conductive anode catalysts in a solid oxide fuel cell for methane internal reforming and partial oxidation, Int. J. Hydrog. Energy 36 (2011) 5632–5643, http://dx.doi.org/10.1016/j.ijhydene.2011.01.163.
[26] E.P. Murray, T. Tsai, S.A. Barnett, A direct-methane fuel cell with a ceria-based anode, Nature 400 (1999) 649–651, http://dx.doi.org/10.1038/23220.
[27] T. Hibino, A. Hashimoto, K. Asano, M. Yano, M. Suzuki, M. Sano, An intermediate-temperature solid oxide fuel cell providing higher performance with hydrocarbons than with hydrogen, Electrochem. Solid-State Lett. 5 (2002) A242–A244, http://dx.doi.org/10.1149/1.1508551.
[28] Z. Zhan, Y. Lin, M. Pillai, I. Kim, S.A. Barnett, High-rate electrochemical partial oxidation of methane in solid oxide fuel cells, J. Power Sources 161 (2006) 460–465, http://dx.doi.org/10.1016/j.jpowsour.2006.04.139.
[29] J.-H. Myung, H.-J. Ko, J.-J. Lee, J.-H. Lee, S.-H. Hyun, Synthesis and characterization of NiO/GDC–GDC dual nano-composite powders for high-performance methane fueled solid oxide fuel cells, Int. J. Hydrog. Energy 37 (2012) 11351–11359, http://dx.doi.org/10.1016/j.ijhydene.2012.04.140.
[30] Y. Chen, Y. Zhang, Y. Lin, Z. Yang, D. Su, M. Han, F. Chen, Direct-methane solid oxide fuel cells with hierarchically porous Ni-based anode deposited with nanocatalyst layer, Nano Energy 10 (2014) 1–9, http://dx.doi.org/10.1016/j.nanoen.2014.08.016.
[31] Y. Lin, Z. Zhan, S.A. Barnett, Improving the stability of direct-methane solid oxide fuel cells using anode barrier layers, J. Power Sources 158 (2006) 1313–1316, http://dx.doi.org/10.1016/j.jpowsour.2005.09.060.
[32] H. Zhu, A.M. Colclasure, R.J. Kee, Y. Lin, S.A. Barnett, Anode barrier layers for tubular solid-oxide fuel cells with methane fuel streams, J. Power Sources 161 (2006) 413–419, http://dx.doi.org/10.1016/j.jpowsour.2006.04.101.
[33] J. Myung, S.-D. Kim, T.H. Shin, D. Lee, J.T.S. Irvine, J. Moon, S.-H. Hyun, Nano-composite structural Ni–Sn alloy anodes for high performance and durability of direct methane-fueled SOFCs, J. Mater. Chem. A 3 (2015) 13801–13806, http://dx.doi.org/10.1039/C4TA06037G.
[34] H. Zhu, W. Wang, R. Ran, Z. Shao, A new nickel–ceria composite for direct-methane solid oxide fuel cells, Int. J. Hydrog. Energy 38 (2013) 3741–3749, http://dx.doi.org/10.1016/j.ijhydene.2013.01.032.
[35] T. Suzuki, T. Yamaguchi, K. Hamamoto, Y. Fujishiro, M. Awano, N. Sammes, A functional layer for direct use of hydrocarbon fuel in low temperature solid-oxide fuel cells, Energy Environ. Sci. 4 (2011) 940–943, http://dx.doi.org/10.1039/C0EE00231C.
[36] K. Wang, R. Ran, Z. Shao, Methane-fueled IT-SOFCs with facile in situ inorganic templating synthesized mesoporous $Sm_{0.2}Ce_{0.8}O_{1.9}$ as catalytic layer, J. Power Sources 170 (2007) 251–258, http://dx.doi.org/10.1016/j.jpowsour.2007.04.030.
[37] D. Yoon, A. Manthiram, Hydrogen tungsten bronze as a decoking agent for long-life, natural gas-fueled solid oxide fuel cells, Energy Environ. Sci. 7 (2014) 3069–3076, http://dx.doi.org/10.1039/C4EE01455C.
[38] B.C.H. Steele, Fuel-cell technology: running on natural gas, Nature 400 (1999) 619–621, http://dx.doi.org/10.1038/23144.
[39] S. Park, J.M. Vohs, R.J. Gorte, Direct oxidation of hydrocarbons in a solid-oxide fuel cell, Nature 404 (2000) 265–267.
[40] Y. Lin, Z. Zhan, J. Liu, S.A. Barnett, Direct operation of solid oxide fuel cells with methane fuel, Solid State Ion. 176 (2005) 1827–1835, http://dx.doi.org/10.1016/j.ssi.2005.05.008.
[41] S. Tao, J.T.S. Irvine, A redox-stable efficient anode for solid-oxide fuel cells, Nat. Mater. 2 (2003) 320–323, http://dx.doi.org/10.1038/nmat871.
[42] Y.-H. Huang, R.I. Dass, Z.-L. Xing, J.B. Goodenough, Double perovskites as anode materials for solid-oxide fuel cells, Science 312 (2006) 254–257, http://dx.doi.org/10.1126/science.1125877.
[43] J.C. Ruiz-Morales, J. Canales-Vázquez, C. Savaniu, D. Marrero-López, W. Zhou, J.T.S. Irvine, Disruption of extended defects in solid oxide fuel cell anodes for methane oxidation, Nature 439 (2006) 568–571, http://dx.doi.org/10.1038/nature04438.
[44] A.T. Ashcroft, A.K. Cheetham, J.S. Foord, M.L.H. Green, C.P. Grey, A.J. Murrell, P.D.F. Vernon, Selective oxidation of methane to synthesis gas using transition metal catalysts, Nature 344 (1990) 319–321, http://dx.doi.org/10.1038/344319a0.
[45] D.A. Hickman, L.D. Schmidt, Production of syngas by direct catalytic oxidation of methane, Science 259 (1993) 343–346, http://dx.doi.org/10.1126/science.259.5093.343.
[46] Y.-H. Chin, C. Buda, M. Neurock, E. Iglesia, Reactivity of chemisorbed oxygen atoms and their catalytic consequences during CH_4–O_2 catalysis on supported Pt clusters, J. Am. Chem. Soc. 133 (2011) 15958–15978, http://dx.doi.org/10.1021/ja202411v.
[47] X. Jacques-Bedard, T.W. Napporn, R. Roberge, M. Meunier, Coplanar electrodes design for a single-chamber SOFC, J. Electrochem. Soc. 154 (2007) B305–B309.
[48] Z. Wang, Z. Lü, B. Wei, K. Chen, X. Huang, W. Pan, W. Su, Redox of Ni/YSZ anodes and oscillatory behavior in single-chamber SOFC under methane oxidation conditions, Electrochim. Acta 56 (2011) 6688–6695, http://dx.doi.org/10.1016/j.electacta.2011.05.053.
[49] D. Lee, D. Kim, J. Kim, J. Moon, Characterizing nano-scale electrocatalysis during partial oxidation of methane, Sci. Rep. 4 (2014) 3937, http://dx.doi.org/10.1038/srep03937.
[50] B.E. Buergler, A.N. Grundy, L.J. Gauckler, Thermodynamic equilibrium of

single-chamber SOFC relevant methane–air mixtures, J. Electrochem. Soc. 153 (2006) A1378–A1385, http://dx.doi.org/10.1149/1.2201546.
[51] T. Hibino, A. Hashimoto, T. Inoue, J. Tokuno, S. Yoshida, M. Sano, A low-operating-temperature solid oxide fuel cell in hydrocarbon-air mixtures, Science 288 (2000) 2031–2033, http://dx.doi.org/10.1126/science.288.5473.2031.
[52] I. Riess, On the single chamber solid oxide fuel cells, J. Power Sources 175 (2008) 325–337, http://dx.doi.org/10.1016/j.jpowsour.2007.09.041.
[53] B. Christian Enger, R. Lødeng, A. Holmen, A review of catalytic partial oxidation of methane to synthesis gas with emphasis on reaction mechanisms over transition metal catalysts, Appl. Catal. Gen. 346 (2008) 1–27, http://dx.doi.org/10.1016/j.apcata.2008.05.018.
[54] R. Jin, Y. Chen, W. Li, W. Cui, Y. Ji, C. Yu, Y. Jiang, Mechanism for catalytic partial oxidation of methane to syngas over a Ni/Al_2O_3 catalyst, Appl. Catal. Gen. 201 (2000) 71–80, http://dx.doi.org/10.1016/S0926-860X(00)00424-5.
[55] W.C. Chueh, Y. Hao, W. Jung, S.M. Haile, High electrochemical activity of the oxide phase in model ceria–Pt and ceria–Ni composite anodes, Nat. Mater. 11 (2012) 155–161, http://dx.doi.org/10.1038/nmat3184.
[56] W. Jung, J.O. Dereux, W.C. Chueh, Y. Hao, S.M. Haile, High electrode activity of nanostructured, columnar ceria films for solid oxide fuel cells, Energy Environ. Sci. 5 (2012) 8682–8689, http://dx.doi.org/10.1039/C2EE22151A.
[57] F. Wang, W. Wang, R. Ran, M.O. Tade, Z. Shao, Aluminum oxide as a dual-functional modifier of Ni-based anodes of solid oxide fuel cells for operation on simulated biogas, J. Power Sources 268 (2014) 787–793, http://dx.doi.org/10.1016/j.jpowsour.2014.06.087.
[58] H.J. Hwang, J.W. Moon, Y.H. Lim, S.H. Lee, E.A. Lee, Fabrication of a strontium-doped lanthanum chromite (LSC) thin film on SUS430 substrate, Key Eng. Mater. 317–318 (2006) 173–176, http://dx.doi.org/10.4028/. www.scientific.net/KEM.317-318.173.
[59] A.F. Carley, S.D. Jackson, J.N. O'Shea, M.W. Roberts, The formation and characterisation of Ni^{3+} — an X-ray photoelectron spectroscopic investigation of potassium-doped Ni(110)–O, Surf. Sci. 440 (1999) L868–L874, http://dx.doi.org/10.1016/S0039-6028(99)00872-9.
[60] A.P. Grosvenor, M.C. Biesinger, R.S.C. Smart, N.S. McIntyre, New interpretations of XPS spectra of nickel metal and oxides, Surf. Sci. 600 (2006) 1771–1779.
[61] F. Bridges, C.H. Booth, M. Anderson, G.H. Kwei, J.J. Neumeier, J. Snyder, J. Mitchell, J.S. Gardner, E. Brosha, Mn K-edge XANES studies of $La_{1-x}A_xMnO_3$ systems (A=Ca, Ba, Pb), Phys. Rev. B 63 (2001) 214405, http://dx.doi.org/10.1103/PhysRevB.63.214405.
[62] W.-S. Dong, K.-W. Jun, H.-S. Roh, Z.-W. Liu, S.-E. Park, Comparative study on partial oxidation of methane over Ni/ZrO_2, Ni/CeO_2 and $Ni/Ce–ZrO_2$ catalysts, Catal. Lett. 78 (2002) 215–222, http://dx.doi.org/10.1023/A:1014905318290.